Computational simulation of microstructure evolution during solidification of ductile cast iron

D. J. Celentano*[1], P. M. Dardati[2], L. A. Godoy[3] and R. E. Boeri[4]

This paper presents a thermomicrostructural model for the simulation of the solidification process of an eutectic ductile cast iron. The thermal balance is written at a macroscopic level and takes into account both the structural component being cast and its mould. Models of nucleation and growth represent the evolution of the microstructure, and the microsegregation of silicon is also considered. The resulting formulation is solved using a finite element discretisation of the macrodomain, in which the evolution of the microstructure is taken into account at the Gauss integration points. The numerical results are presented in terms of cooling curves and are compared with available experimental values. Furthermore, the sensitivity of the response with respect to changes in the cooling rate and nucleation parameters are investigated. The agreement between experimental and computational values is acceptable in both quantitative and qualitative aspects. Ways to improve the computational model are suggested.

Keywords: Finite elements, Microstructure evolution, SG cast iron, Solidification, Thermal model

Introduction

This paper presents a simulation of the solidification processes of spheroidal graphite (SG) cast iron by means of a coupled macro–micromechanical formulation.

Spheroidal graphite cast iron, also known as ductile cast iron, nodular iron, or ductile iron, plays a key role in metallurgical industries and in some engineering processes. Because of its advantageous mechanical properties, SG cast iron has substituted cast steel and forged steel in a number of applications. The new feature is that the spherical structure of graphite can be obtained as a result of the solidification process instead of the long and expensive thermal treatments that are needed following the solidification of white cast iron. However, the mechanisms involved in the formation of SG cast iron are not simple, and there have been many attempts to explain this process. The main difficulties to build a satisfactory model are associated to a lack of empirical evidence about what exactly occurs during solidification. The importance of simulation in this field of science and engineering cannot be overstated. There are tremendous difficulties in the experimental work, which would be the subject of a paper itself, mainly because one needs to investigate a process without full access to it, and also because any measuring device interferes with the very process that it is trying to investigate. Simulation by itself, on the other hand, cannot proceed because there is a strong need to have evidence regarding the evolution of the microstructure. Thus, it seems clear that further advances in this field require both experimental evidence and computational simulation of the process, in which the latter may help to understand the consequences of the assumptions made in the physical theories.

In this paper, the macro problem is solved as a continuous media using a finite element model for heat transfer with latent heat generated by the phase change. The formulation considers changes in thermal properties of the material due to temperature variations, and assumes that conductivity is a function of the state of the material (either liquid, solid or mushy). At the microscopic level the solidification of SG cast iron is modelled by means of a multinodular theory, in which there are explicit laws for nucleation and growth of graphite and lever rules for austenite. The micro problem includes effects due to microsegregation of silicon. The two levels (macro and micro) are coupled at Gauss integration points in the finite element discretisation. The computer implementation carried out is independent of the specific model used to represent the micro problem and may serve as a platform to compare different assumptions made at a more physical level.

Main assumptions about solidification process

At present, most researchers agree that graphite nucleates directly in the liquid, but some points of

[1]Departamento de Ingeniería Mecánica y Metalúrgica, Pontificia Universidad Católica de Chile, Santiago de Chile, Chile
[2]Departamento Ingeniería Mecánica y CIII, Facultad Regional Córdoba, Universidad Tecnológica Nacional, Córdoba, Argentina
[3]Departamento de Estructuras, Facultad de Ciencias Exactas, Físicas y Naturales, Universidad Nacional de Córdoba, Córdoba y CONICET, Argentina
[4]INTEMA, Facultad de Ingeniería, Universidad de Mar del Plata y CONICET, Argentina

*Corresponding author, email dcelentano@ing.puc.cl

Received 1 August 2007; accepted 23 September 2008
DOI 10.1179/136404608X370756

discrepancy still exist, mainly regarding the role of eutectic austenite. Some authors (*see* for example Ref. 1) distinguish between uninodular and multinodular models of the solidification of SG cast iron. Uninodular models assume a basic unit of solidification formed by a graphite nodule and an austenite shell covering the nodule.[2] The multinodular models assume that each unit of solidification is formed by a grain of dendritic austenite containing several graphite spheres. The main postulates of the multinodular theory may be seen in Refs. 3–5.

Most analytical and computational models for the solidification of SG cast iron employ the classical uninodular approach, in which austenite has a spherical growth on top of the graphite nodule.[2,6–13] The multinodular theory, on the other hand, leads to more complex models because of the dendritic growth of austenite. This additional difficulty may explain why the younger nodular theory has not yet been fully explored by computer simulation, although several researchers agree on the dendritic nature of the eutectic austenite.[3–5,14–21] This paper attempts to advance a step further in this direction by reporting an implementation and results for some simple solidification problems.

Thermal–macrostructural formulation

Most previous works modelling a solidification process have been implemented at the macro level (for example, *see* Ref. 22 and 23). To model the cooling of a cast part limited to heat propagation by conduction, the energy equation may be used

$$\rho c\dot{T} = \nabla(k\nabla T) \tag{1}$$

where ρ is the density, c is the specific heat, k is the thermal conductivity, T is the temperature, ∇ the gradient operator, and a dot on top of a variable indicates time derivatives. The solution of this equation should be achieved together with initial and boundary conditions.

To account for phase changes during the cooling process, a new term should be added to equation (1) in the form

$$\rho c\dot{T} + \rho L\dot{f}_{pc} = \nabla(k\nabla T) \tag{2}$$

where L is the specific latent heat of phase change, and f_{pc} is the phase change function with values between zero and one ($0 \leqslant f_{pc} \leqslant 1$). Equation (2) represents a nonlinear problem, on account of the changes that take place in material parameters with temperature evolution. The solution is carried out by means of a space discretisation using the finite element method and a time discretisation using the finite difference method, based on Ref. 22 and 23.

In solidification processes, the function of phase change f_{pc} is given as (1-f_s), where f_s is the solid fraction. In a macroscopic analysis of phase change, f_{pc} is an explicit function of temperature and this is the only independent variable of state in the problem, so that $\dot{f}_{pc}$ may be replaced by $\frac{\partial f_{pc}}{\partial T}\dot{T}$. Such macro models cannot predict microstructural parameters for the different phases that are formed during solidification, such as grain size, eutectic or dendritic spacing, type of microstructure, percentage of microstructural components, and others that may be of interest to engineers or researchers.

The microstructural models formulated in the field of metal solidification usually do not provide a phase change function in explicit form, but deal with its time variation as a function of rates of several independent state variables. For equiaxial solidification, it is possible to write

$$\dot{f}_s = A_N\dot{N} + A_R\dot{r} \tag{3}$$

where N is the grain density and r is the average grain radius. The time derivative of r is the growth rate.

Different authors have different formulations for nucleation (which may be continuous, instantaneous, etc.), and for the growth rate (which may include diffusion of solute, may depend on undercooling, etc.), but in all cases this constitutes a non-linear problem at the micro level.

The coupling of the macro and micro problems is made within the same time and domain discretisation. As time is increased, the results of the macro solution are transferred to the micro level, which is solved and returns the relevant parameters to the macro level before a new time increment is allowed.

Microstructural model for SG cast iron

In this paper the simulation of the micro process is assumed to occur over a representative volume element (RVE) of the microstructure. This constitutive model takes the temperature computed at the macro level at the Gauss integration points, assumes this as a uniform temperature over the RVE, and obtains the evolution of the microstructure. The function of phase change f_{pc} is computed at the RVE and assumed to be an approximate value for the macro problem at the Gauss points in each finite element. The micro constitutive model is based on a multinodular theory, in which stable equiaxial solidification of a nodular cast at an eutectic composition is considered. Furthermore, the microsegregation of silicon is included in the model, so that the composition of the liquid needs to be updated during the process. Finally, the model considers that interaction among grains affects the growth rate, mainly during the final stages of solidification.

Composition of interfaces

The present model considers the solidification of an eutectic cast, so that the growth of primary austenite or graphite is not considered. To account for the influence of Si, the ternary equilibrium diagram Fe–C–Si is used in the form of a two-dimensional diagram, in which the lines of liquidus, solidus, and temperature of eutectic equilibrium are defined by functions that depend on the contents of silicon and carbon in the cast as[24]

$$\begin{aligned} T_{AL} &= 1569 - 97{\cdot}3\left(C + \frac{1}{4}Si\right) \\ T_{AS} &= 1528 - 177{\cdot}9(C + 0{\cdot}18Si) \\ T_{GL} &= 389{\cdot}1\left(C + \frac{1}{3}Si\right) - 503{\cdot}2 \\ T_E &= 1154{\cdot}6 + 6{\cdot}5Si \end{aligned} \tag{4}$$

where the meaning of the temperatures T_{AL}, T_{AS}, T_{GL} and T_E are identified in Fig. 1.

The point of maximum carbon solubility in austenite at eutectic temperature is given by the intersection

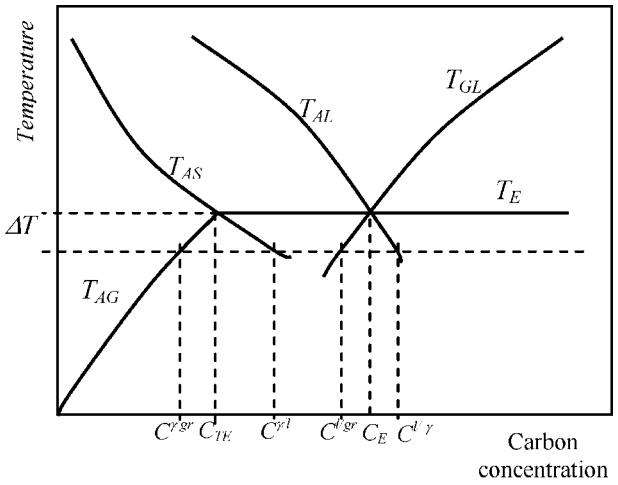

1 Schematic view of eutectic region of Fe–C–Si equilibrium diagram for given Si concentration

between T_{AS} and T_E, and yields

$$C_{TE} = 2{\cdot}1 - 0{\cdot}216Si \tag{5}$$

The contents of eutectic carbon is obtained at the intersection between T_{AL} y T_E

$$C_E = 4{\cdot}26 - 0{\cdot}317Si \tag{6}$$

From equations (5) and (6) it is possible to obtain the percentage of carbon at the interface corresponding to each phase and each temperature in the form

$$C^{l/\gamma} = \frac{1}{97{\cdot}3}(1569 - T - 24{\cdot}32Si)$$

$$C^{\gamma/l} = \frac{1}{177{\cdot}9}(1528{\cdot}4 - T - 32Si)$$

$$C^{l/gr} = \frac{1}{389{\cdot}1}(T - 129{\cdot}7Si + 503{\cdot}2) \tag{7}$$

To define the line T_{AG}, which identifies the variation of the solubility of carbon in austenite in solid state, the point with coordinates 800°C and 0·6%C (assumed as the eutectoid point) is located and joined with C_{TE}, and yields

$$C^{\gamma/gr} = \frac{(T - 1154{\cdot}6 - 6{\cdot}5Si)(1{\cdot}5 - 0{\cdot}216Si)}{(354{\cdot}6 + 6{\cdot}5Si)} + 2{\cdot}1 - 0{\cdot}216Si \tag{8}$$

The curves in Fig. 1 are continued below the eutectic temperature, so that if the temperature descends below the temperature of eutectic and solidification is still occurring, then the lines extrapolated are used to estimate the carbon concentrations of the different phases at the interfaces. Thus, it is assumed that equilibrium conditions are valid in other parts of the volume.

Microsegregation

Contrary to what happens in the solidification of pure metals, the solid and the liquid in alloys have different compositions. This is because the process of phase change from liquid to solid does not occur at a constant temperature but takes place at a range of temperatures in which the composition of liquid to solid in equilibrium changes. Thus, at the end of the process there is a non-uniform distribution of solute in the solid which is known as segregation. In this model the microsegregation of silicon is taken into account by means of a partition coefficient k_{si} which establishes a relation between the concentration of silicon in solid and the concentration of solute in liquid; and by the Scheil equation, which evaluates the percentage of solute in liquid by assuming zero diffusion in solid and uniform composition in liquid

$$Si = Si_0(1 - f_s)^{k_{si}-1} \tag{9}$$

where Si_0 is the percentage of initial silicon.

Graphite nucleation

The exponential law

$$\dot{N} = b\Delta T \exp\left(-\frac{c}{\Delta T}\right) \tag{10}$$

for continuous nucleation is assumed as in Ref. 16, in which the parameters b and c depend on the composition of the cast and on the inoculation treatment affecting the liquid; and $\Delta T = T_E - T$ is the liquid undercooling. The nucleation is assumed to stop when recalescence begins. Recalescence is an effect that may occur if the velocity of production of latent heat due to phase change is higher than the heat extraction.

The velocity of nucleation is assumed to be low until a critical undercooling is reached, and a large increment in the velocity of nucleation occurs beyond that critical point. The expression (10) is changed by[16]

$$\dot{N} = b\Delta T \exp\left(-\frac{c}{\Delta T}\right)(1 - f_s) \tag{11}$$

where the factor $(1-f_s)$ takes into account that the proportion of liquid decreases.

A continuous nucleation generates nodules at different times during the cooling process, and this produces different grain sizes at the end of solidification. The computational storage of the distribution of grain sizes employs two matrices, one to store the number of nodules nucleated at each time step and each point, and another to store the size of the nodules as they grow.

Growth of graphite nodules

This model postulates that nucleation and the early stages of the growth of graphite occur in direct contact with liquid. At a later stage the nodules are reached and encapsulated by austenite dendrites.

To consider the growth of graphite in contact with liquid, the present model employs Zener's equation for the growth of an isolated spherical particle in a matrix with low supersaturation in the form

$$r^2 = \frac{C^{l/\gamma} - C^{l/gr}}{C_{gr} - C^{l/gr}} \frac{\rho_l}{\rho_{gr}} D_c^l t \tag{12}$$

where r is the radius of the graphite sphere; t is the time; D_c^l is the carbon diffusion coefficient in liquid; ρ_γ is the austenite density; ρ_{gr} is the graphite density; $C^{l/\gamma}$ is the carbon concentration of the liquid in equilibrium with austenite; $C^{l/gr}$ is the carbon concentration in liquid in contact with graphite; and C_{gr} is the carbon concentration in graphite. This form of growth is assumed to occur until the nodulus reaches a radius of 6 μm. Then it is assumed that graphite is reached by a dendritic austenite that encloses the graphite, so that further

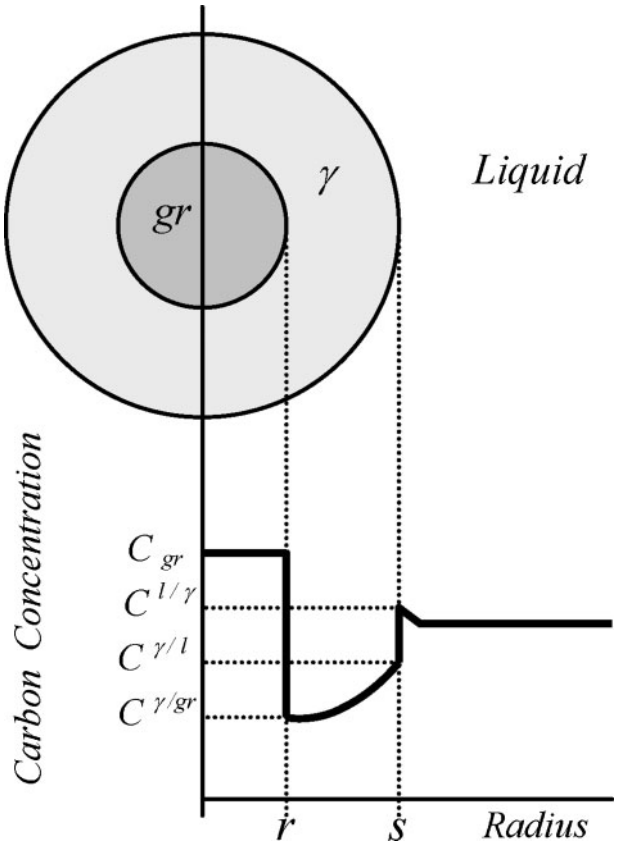

2 Carbon concentration in graphite nodule and austenite shell

growth is due to carbon diffusion from liquid to graphite through austenite.

The growth of graphite in contact with austenite is based on a quasi-stationary process proposed by Su *et al.*[2]

$$\dot{r}=\frac{(C^{\gamma/l}-C^{\gamma/gr})}{(C_{gr}-C^{\gamma/gr})}\frac{\rho_\gamma}{\rho_{gr}}D_c^\gamma\frac{(1-f_s)^{2/3}}{r\left(1-\frac{r}{s}\right)} \tag{13}$$

where s is the radius of the austenite shell, illustrated in Fig. 2; and the interaction between grains is taken into account by the factor $(1–f_s)^{2/3}$.

According to the multinodular theory, austenite does not form a spherical shell (*see* Fig. 3), so that only the thinner parts of the shell contribute to graphite growth by diffusion; to account for this feature, the rate of growth $\dot{r}$ is multiplied by a coefficient 0·9. Furthermore, there is experimental evidence[16] that the ratio between the radius of austenite and graphite is approximately constant and may be taken as 1·89.

Thus, the modified model for $\dot{r}$ becomes

$$\dot{r}=1{\cdot}911\frac{(C^{\gamma/l}-C^{\gamma/gr})}{(C_{gr}-C^{\gamma/gr})}\frac{\rho_\gamma}{\rho_{gr}}D_c^\gamma\frac{(1-f_s)^{2/3}}{r} \tag{14}$$

The model assumes that the ratio between the amount of austenite and graphite is independent of undercooling and remains constant during growth for each silicon concentration. Using the lever rule in the conditions of eutectic equilibrium, this ratio is

$$REAG(\%)=\frac{100-C_E}{C_E-C_{TE}} \tag{15}$$

The graphite fraction in a specific volume element f_{gr} is

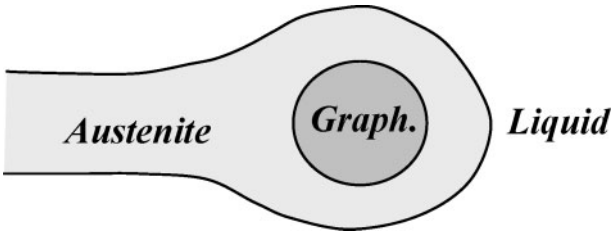

3 Graphite nodule enclosed by austenite

$$f_{gr}=\sum_1^k\frac{4}{3}\pi N_k r_k^3 \tag{16}$$

where k is the number of different nodular radii that are present in a volume element due to the non-simultaneity of nucleation. The austenite fraction is computed as

$$f_\gamma=REAG f_{gr} \tag{17}$$

while the solid fraction is given by

$$f_s=f_{gr}(1+REAG) \tag{18}$$

This value of f_s is next returned to the macro problem to continue with the solution of equation (2). This completes the microstructural model, and the following sections report results obtained from computational simulations.

A computational flow diagram followed in this work to evaluate the microstructural model is included in Appendix A.

Sensitivity analysis of microstructural model

Influence of nucleation parameters *b* and *c*

According to equation (11), the nucleation process depends on two parameters b and c, which should be evaluated experimentally. However, in order to understand the influence of both parameters on the response, sensitivity analyses are carried out in this section. The study is performed on a single finite element modelling ductile iron, under unidirectional thermal flow, and with a constant rate of heat extraction.

The results of Fig. 4 illustrate that, as the value of b is increased, there is a decrease both in undercooling and in recalescence amplitude. This is an expected behaviour because as the number of nodules that nucleate and grow increases, the latent heat generated equilibrates faster the heat flow being extracted, which is constant in the present parametric study.

The total solidification time increases with a decrease in the value of b (Fig. 5). As expected, the final number of graphite nodules in Fig. 6*a* increases with b, whereas the maximum size of graphite nodules decreases (Fig. 6*b*).

An increase in c is responsible for an increase in undercooling and recalescence, as shown in Fig. 7. On the other hand, Fig. 8 shows that changes in c do not significantly affect the solidification time; an increase in c decreases the final number of nodules per unit volume (Fig. 9*a*); and an increase in c also increases the maximum size of graphite spheres (Fig. 9*b*).

Influence of cooling rate

To a large extent, the final microstructure of the SG cast iron depends on the cooling rate. Such influence would

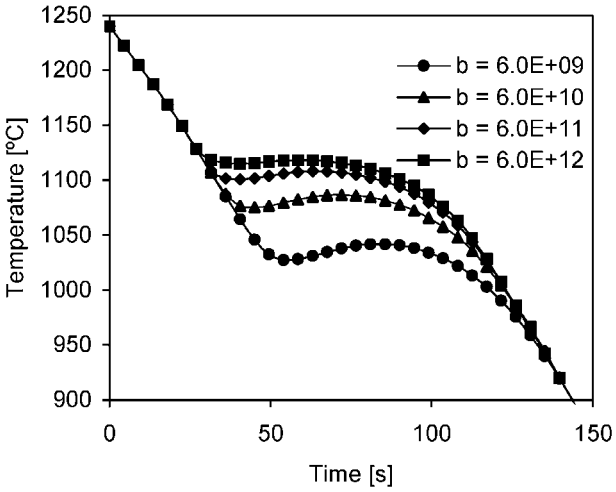

4 Cooling curves for different values of nucleation parameter *b*

not be detected by a macrostructural model because the 'solidification path', given by the f_s–T curve, is unique in this case.[22,23] In a real situation, the cooling rate depends on a combination of several factors, such as the size and characteristic features of the mould, environmental conditions, and cast temperature. In this simple example, the cooling rate is changed by means of a change in the heat extraction rate q. As q increases, the results in Fig. 10 show an increase in the slope of the cooling curves and a decrease in the longitude of the plateau. Solidification time increases as q is reduced (Fig. 11). Other observations which are in agreement with experimental evidence[19–21] are an increase in the number of nodules per unit volume with an increase in the cooling rate (Fig. 12*a*); and a decrease in the maximum size of spheres (Fig. 12*b*).

Validation of model using experimental evidence

One of the difficulties encountered by researchers to assess the quality of models in SG cast iron is the lack of experimental evidence available in the literature. Experiments in this field are expensive, time consuming, and subject to various uncertainties, so that the difficulties of the task tend to discourage many

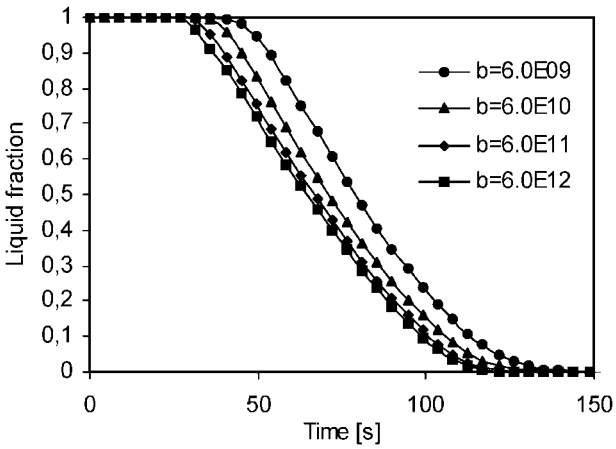

5 Liquid fraction evolution for different values of nucleation parameter *b*

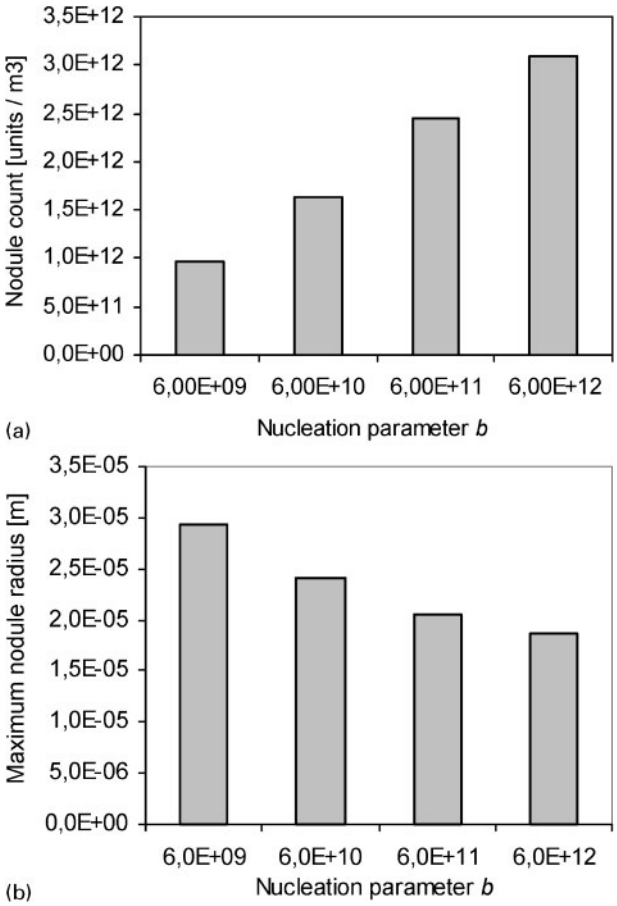

6 *a* nodule count for different values of nucleation parameter *b* and *b* maximum nodule radius for different values of nucleation parameter *b*

experimentalists. In this case, results of the model have been compared with carefully controlled experiments carried out by one of the authors[16] for the solidification of ductile cast iron with eutectic composition on a cylindrical sand mould. The properties of the material and the geometry are shown in Fig. 13 and Table 1. A heat transfer coefficient of 100 W m^{-2} $°C^{-1}$ was considered to model the heat convection to the environment. The temperature was measured in two points at the same elevation, one on the axis of the coupon and a second one on the boundary in contact with sand.

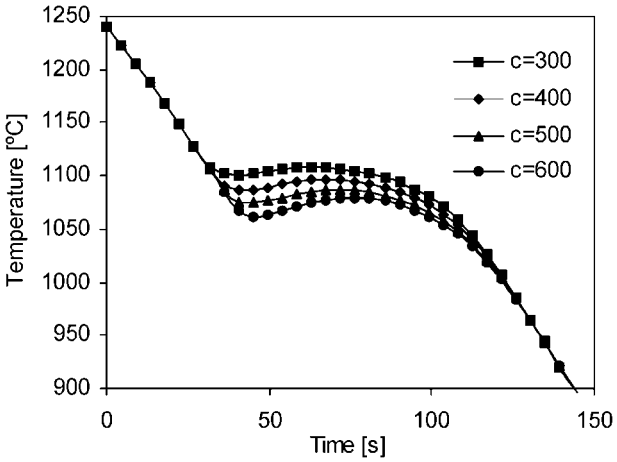

7 Cooling curves for different values of nucleation parameter *c*

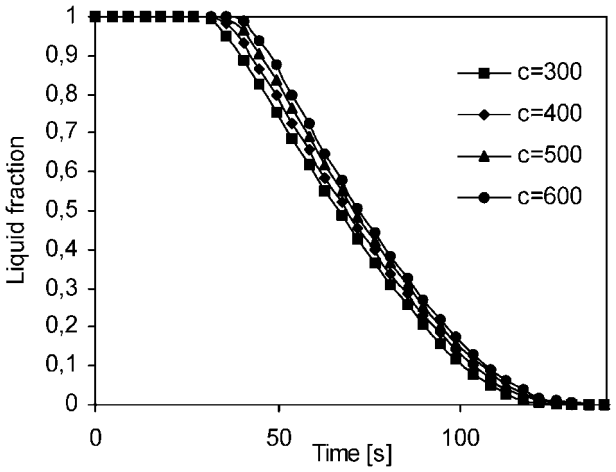

8 Liquid fraction evolution for different values of nucleation parameter *c*

Because of the cylindrical nature of the problem, then it is possible to use an axisymmetric model. The discretisation of the geometry was carried out by means of 5190 two-dimensional four node finite elements for axisymmetric solids.

The results are plotted in Fig. 14 in a graph of temperature versus time. Solid lines represent the computations using this model, whereas dots indicate experimental results from Ref. 16. Good qualitative agreement is found, together with a reasonable quantitative approximation to the experiments.

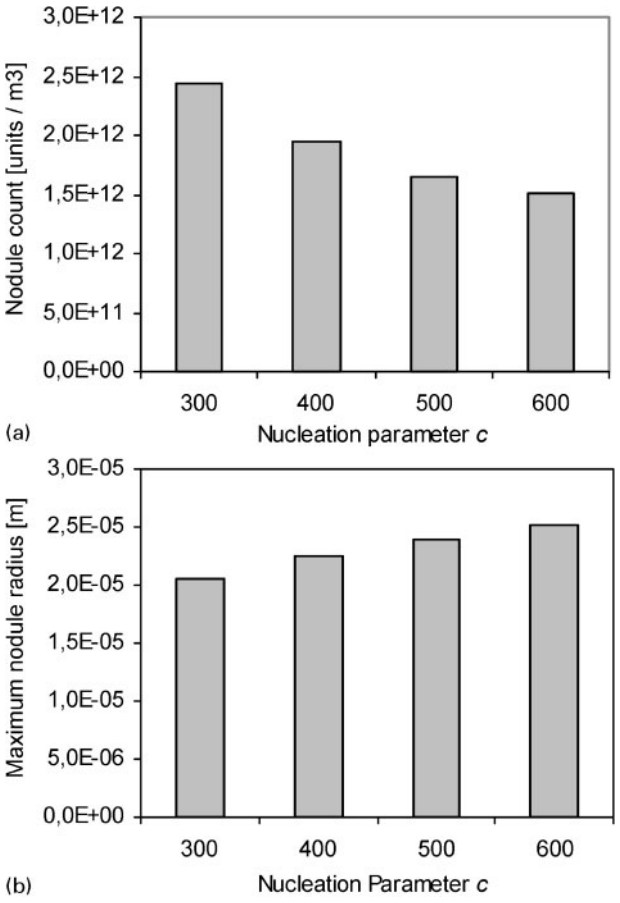

9 *a* nodule count for different values of nucleation parameter *c* and *b* maximum nodule radius for different values of nucleation parameter *c*

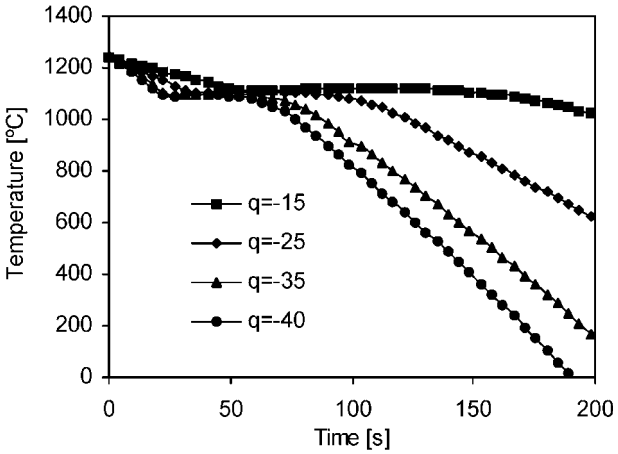

10 Cooling curves for different values of heat extraction rate *q*

At the onset of the process, the curve corresponding to the point on the outer face of the coupon has a higher slope than that obtained for the point at the central axis (Fig. 14), because of the different rates of heat transfer. There is a noticeable plateau in the curve corresponding to the central point in both computations and experiments; this plateau is less evident at the point on the outer face of the coupon. At the end of the process both experimental and computational curves become very close to each other. The only significant differences are observed at the beginning of the process; this must be associated to the questionable theoretical assumptions that the mould is filled instantaneously and that the initial temperature is uniform in all points. Other sources of discrepancies may be the inertia in the thermocouples employed in the experiments, a small error in starting measuring the time and problems of contact between thermocouples and material under solidification. Thus, it is possible that a better agreement would be found if such errors were corrected. But on the whole, the present model is capable of representing accurately the behaviour during the solidification process.

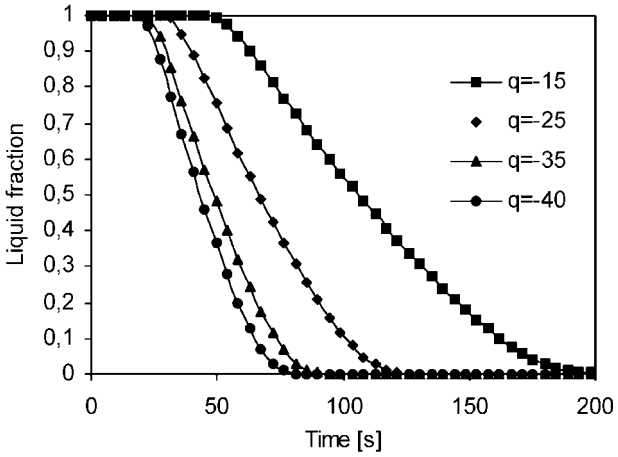

11 Liquid fraction evolution for different values of heat extraction rate *q*

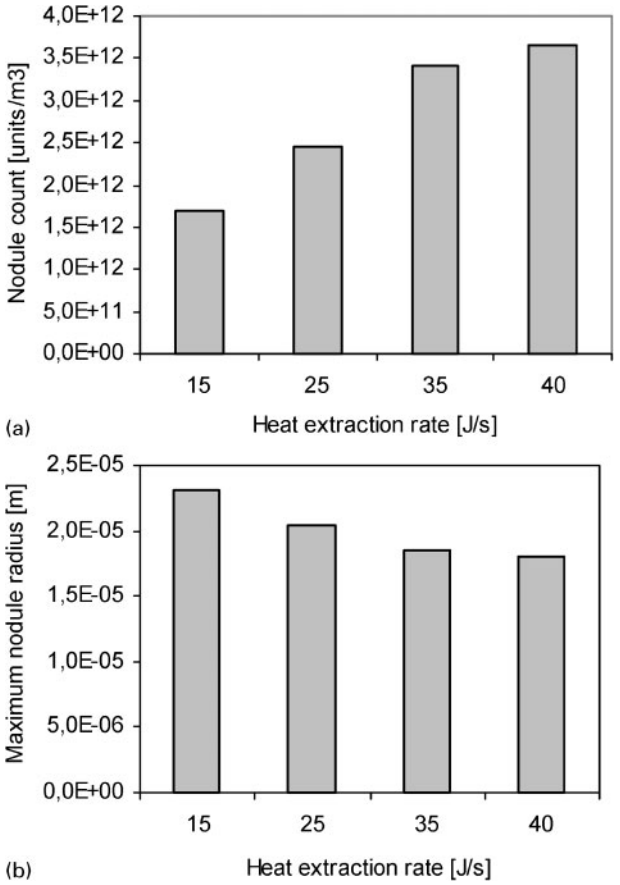

12 ***a*** **nodule count for different values of heat extraction rate** ***q*** **and** ***b*** **maximum nodule radius for different values of heat extraction rate** ***q***

Comparison between two and one-dimensional models

Because the length of the coupon is several times its width, then the heat flow at the central part of the coupon is almost unidirectional in the radial direction. The bidimensional nature of the problem is only reflected near the bottom and top edges, so that a one-dimensional model may be employed to model the response at the central part of the coupon. Thus, a one-dimensional discretisation was carried out with 92 axisymmetric elements.

A comparison between cooling curves computed using two-dimensional and one-dimensional models is presented for a point on the central axis and a point on the surface of the coupon (Fig. 15). In both cases the curves are close to each other.

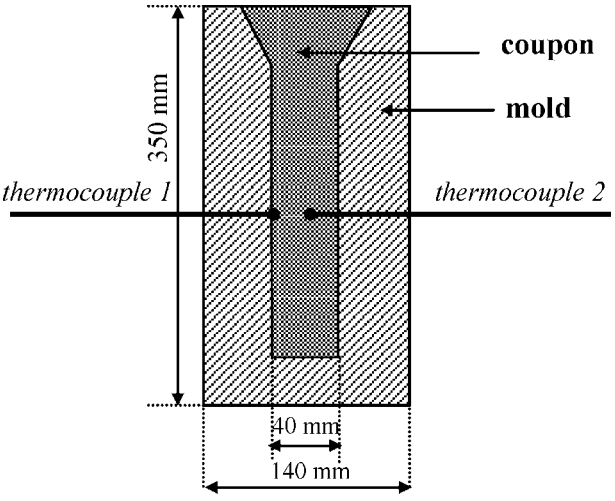

13 Geometry of coupon and mould

Figure 16 shows a comparison of the evolution of the liquid austenite and graphite fraction obtained for one and two-dimensional analysis, at a point located halfway between the central axis and the external surface. Both models compute the same total time for solidification and the same final fractions of both austenite and graphite.

Comparison between microstructural models

It was mentioned before that the computer implementation of this problem has been conducted in such a way that different microstructural models can be implemented with ease. A second model due to Su *et al.*,[2] which follows the uninodular theory, was also implemented. The main features of this uninodular model are:

(i) nucleation stops with recalescence and may be obtained from the condition

$$\dot{N} = A\Delta T^{n} \tag{19}$$

where A is a nucleation parameter, and the exponent n may take values of 1 or 2. In this paper, values of $A=8{\cdot}1\text{E}07$ and $n=2$ have been adopted

(ii) at the beginning of nucleation, it is assumed that graphite is enclosed by austenite, so that graphite does not grow in contact with liquid. The initial conditions of the nucleus are graphite radius $r=1$ μm and austenite radius $s=1{\cdot}2$ μm

Table 1 Material properties

Ductile iron properties	
Thermal conductivity, W m^{-1} °C^{-1}	solid=30, mushy=25, liquid=30
Density, kg m^{-3}	7000
Specific heat, kJ kg^{-1} °C^{-1}	$cp=0{\cdot}61+1{\cdot}214\times10^{-4}\times T$ for 777°C$<T\leqslant$1130°C $cp=0{\cdot}915$ for $T>$1130°C
Latent heat, kJ kg^{-1}	185
Diffusion coefficient of C, m^2 s^{-1}	in liquid$=5{\cdot}0\times10^{-10}$ in austenite$=9{\cdot}0\times10^{-11}$
Nucleation parameters	$b=9{\cdot}0\times10^{11}$ $c=250$
Sand properties	
Thermal conductivity, W m^{-1} °C^{-1}	1·1
Density, kg m^{-3}	1500
Specific heat, kJ kg^{-1} °C^{-1}	$cp=0{\cdot}782+5{\cdot}71\times10^{-4}\times T-1{\cdot}88\times10^{-4}\times T^{-2}$ for $T\leqslant$846 K $cp=1{\cdot}00+1{\cdot}35\times10^{-4}\times T$ for $T>$846 K

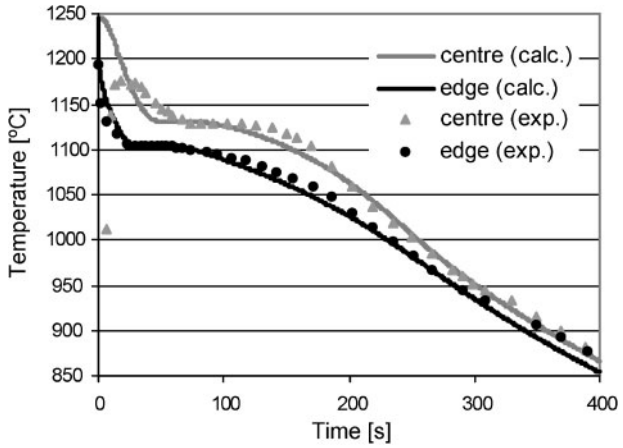

14 Calculated and measured cooling curves at casting centre and at casting edge

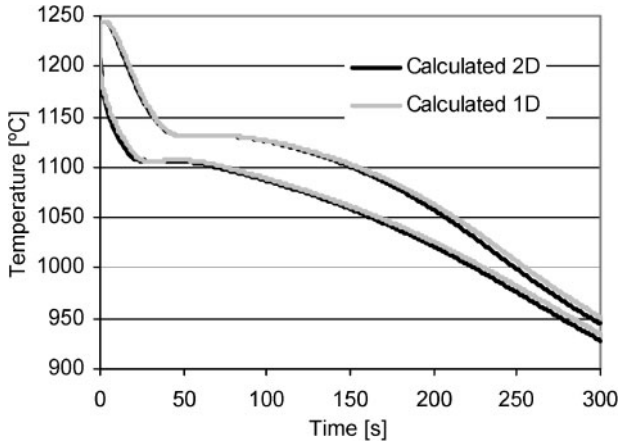

15 Calculated cooling curves by one and two-dimensional models at casting centre and at casting edge

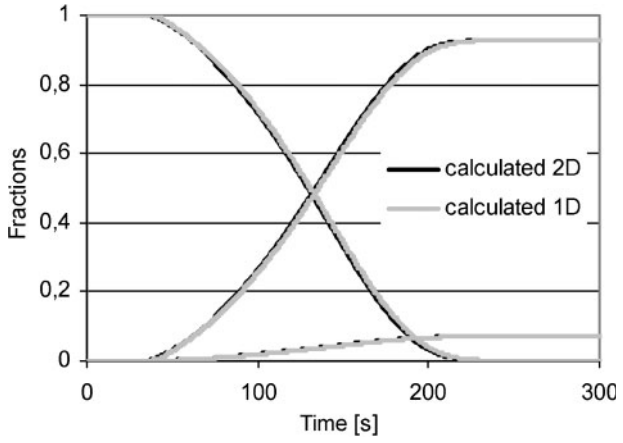

16 Calculated liquid, evolution of austenite and graphite fractions computed with one and two-dimensional models

(iii) the radius s of the spherical austenite grows according to the following law

$$\dot{s} = \frac{(C^{\gamma/l} - C^{\gamma/gr})}{(C^{l/\gamma} - C^{\gamma/l})} \frac{D_c^{\gamma}}{s\left(\frac{s}{r} - 1\right)} \left(\frac{1 - f_s}{1 - 0{\cdot}5}\right)^{2/3} \quad (20)$$

(iv) the radius r of a graphite nodule is assumed to grow in the form

$$\dot{r} = \frac{(C^{\gamma/l} - C^{\gamma/gr})}{(100 - C^{\gamma/gr})} D_c^{\gamma} \frac{\rho_{\gamma}}{\rho_{gr}} \frac{r}{\left(1 - \frac{r}{s}\right)} \quad (21)$$

(v) finally, the original model published by Su *et al.*[2] does not consider silicon segregation; however, such segregation was included in the present implementation in order to have a more meaningful comparison of the laws of nucleation and growth.

Cooling curves were computed for both uninodular and multinodular models using a one-dimensional discretisation, and the results are shown in Fig. 17. The results indicate that the uninodular model has a more severe undercooling and recalescence; this behaviour is associated with the nucleation laws employed by the model. The differences in the rest of the process between the values of both models are difficult to explain because they are influenced by the values in the early stages.

Modified nucleation conditions

Many of the models proposed by researchers in this field identify the end of nucleation with the beginning of recalescence. However, there is some empirical evidence that new graphite nodules may nucleate during the remaining time of the solidification process.[2,3,25] This motivated a new analysis of the cylindrical coupon using the multinodular model but including changes in the nucleation conditions, so that nucleation stops at the initiation of recalescence but starts again when the temperature becomes lower than the lowest temperature reached if solidification has not yet finished. The new results are shown in Fig. 18 together with experiments, and it may be seen that better agreement is obtained at the end of the plateau.

In order to explore how well the multinodular model predicts the solidification behaviour of ductile cast iron with eutectic composition for other casting conditions with respect to those considered in the problem shown in Fig. 13, a second experiment with a larger sample diameter leading to significantly different cooling rates was also analysed (it should be mentioned that the composition of the cast and the inoculation treatment were the same as those considered in the previous problem). The experimental set-up of this problem,

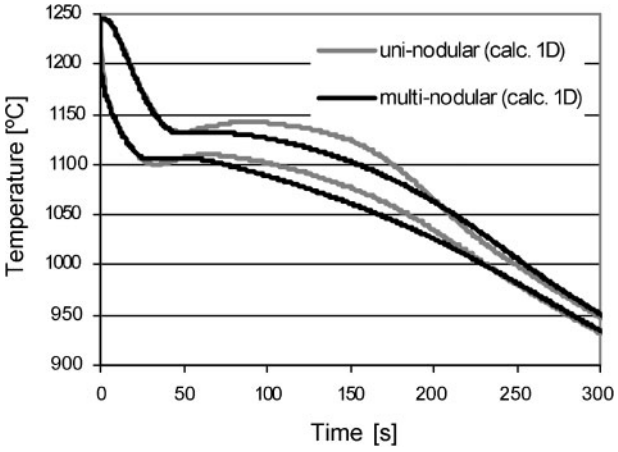

17 Cooling curves calculated by a uninodular model and a multinodular model at casting centre and at casting edge

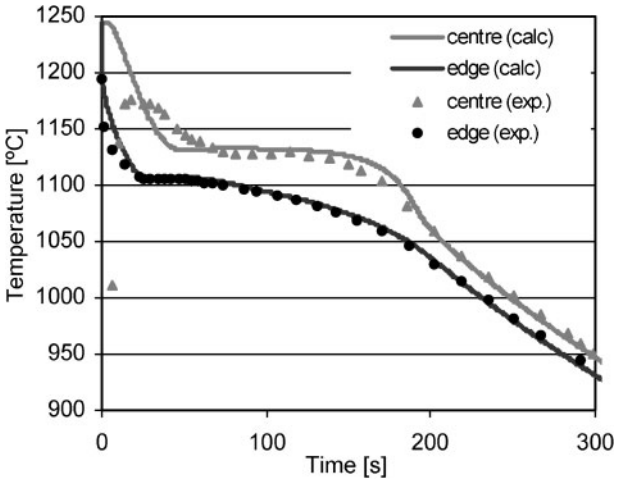

18 Cooling curves calculated with multinodular model (with modified nucleation) at casting centre and at casting edge

performed by one of the authors and reported in detail in Ref. 16, is sketched in Fig. 19. The melt was poured into a resin coated silica sand mould. The sand mould was contained in a steel flash to prevent expansion or cracking of the mould due to the large stresses generated in the mould as the graphite nodules precipitate and grow in the ductile iron. The melt was solidified primarily from the vertical side walls of the mould. This was achieved by placing a refractory brick next to the vertical walls to increase the radial heat flow. Water forced cooling was achieved by placing a copper coil 10 mm from the vertical surfaces of the mould. The diameter of the tube was 10 mm. After pouring, the top was covered by a lid made of refractory brick. Temperatures during cooling were measured with three thermocouples placed at the positions shown in Fig. 19.

The simulation of this problem was carried out with a one-dimensional discretisation composed of 73 axisymmetric elements. For simplicity, the inner part of the mould is only discretised considering a wall thickness of 10 mm. The initial casting temperature was 1245°C while the temperature of the external surface of the mould was assumed as 25°C. Although the material properties shown in Table 1 were also essentially considered in this analysis, larger values for the conductivity in the liquid phase and the heat transfer coefficient were adopted in the present simulation (80 W m^{-1} $°C^{-1}$ and 200 W m^{-2} $°C^{-1}$ respectively) to take into account two particular features of this

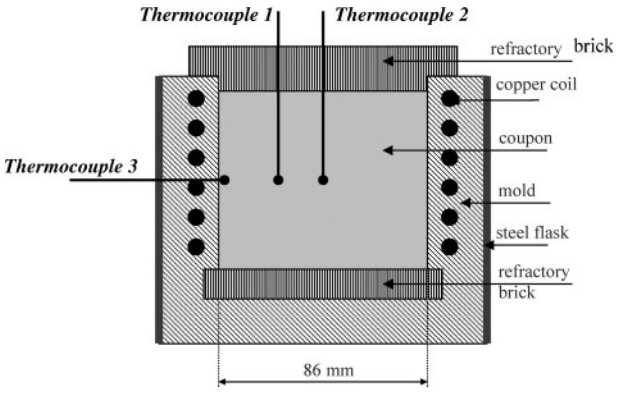

19 Geometry of coupon and water forced cooled mould

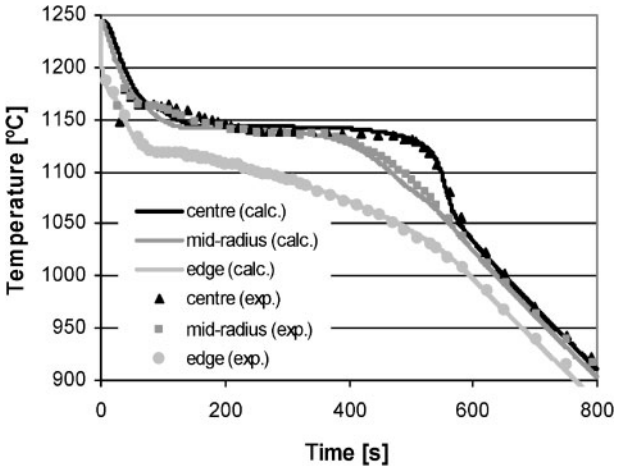

20 Calculated and measured cooling curves at casting centre, at casting mid radius and at casting edge for water forced cooled mould problem: numerical predictions were obtained with multinodular model (with modified nucleation)

problem: the expected development of higher natural convection effects due to the increase in the diameter of the coupon and the presence of water forced cooling conditions.

The calculated and measured cooling curves at the different locations are presented in Fig. 20. The numerical predictions were obtained with a multinodular model with modified nucleation. Once again, a very good agreement between the experimental and computed results can be appreciated. Therefore, this second problem serves as verification of the microstructural model response under different cooling rates and, in addition, ratifies the consistent choice of the adopted nucleation parameters.

Conclusions

A new computational model has been presented in this paper in which a heat problem has been coupled with the microstructural evolution of SG cast iron. The model simulates the cooling and solidification processes in SG cast iron with eutectic composition using a multinodular theory for nucleation and growth. The main conclusions of the study may be summarised as follows.

1. The exponential nucleation law used in the model includes two parameters b and c, and variations of those parameters change important aspects of cooling curves, such as undercooling and recalescence, the number and final size of nuclei, and the total time of solidification. The parameter c has a direct influence on undercooling and recalescence amplitude, while b has an inverse influence. An increase in b increases the final number of nodules but reduces the nodule size, while an increase in c produces the opposite effect.

2. The numerical results have been validated by comparison with experimental evidence. A good qualitative agreement was found between theory and experiments, with some differences obtained in the cooling curves at the beginning of the process.

3. The multinodular approach investigated in this paper has been compared with a uninodular model available in the literature and implemented in the same code, and the results of the latter are seen to depart from

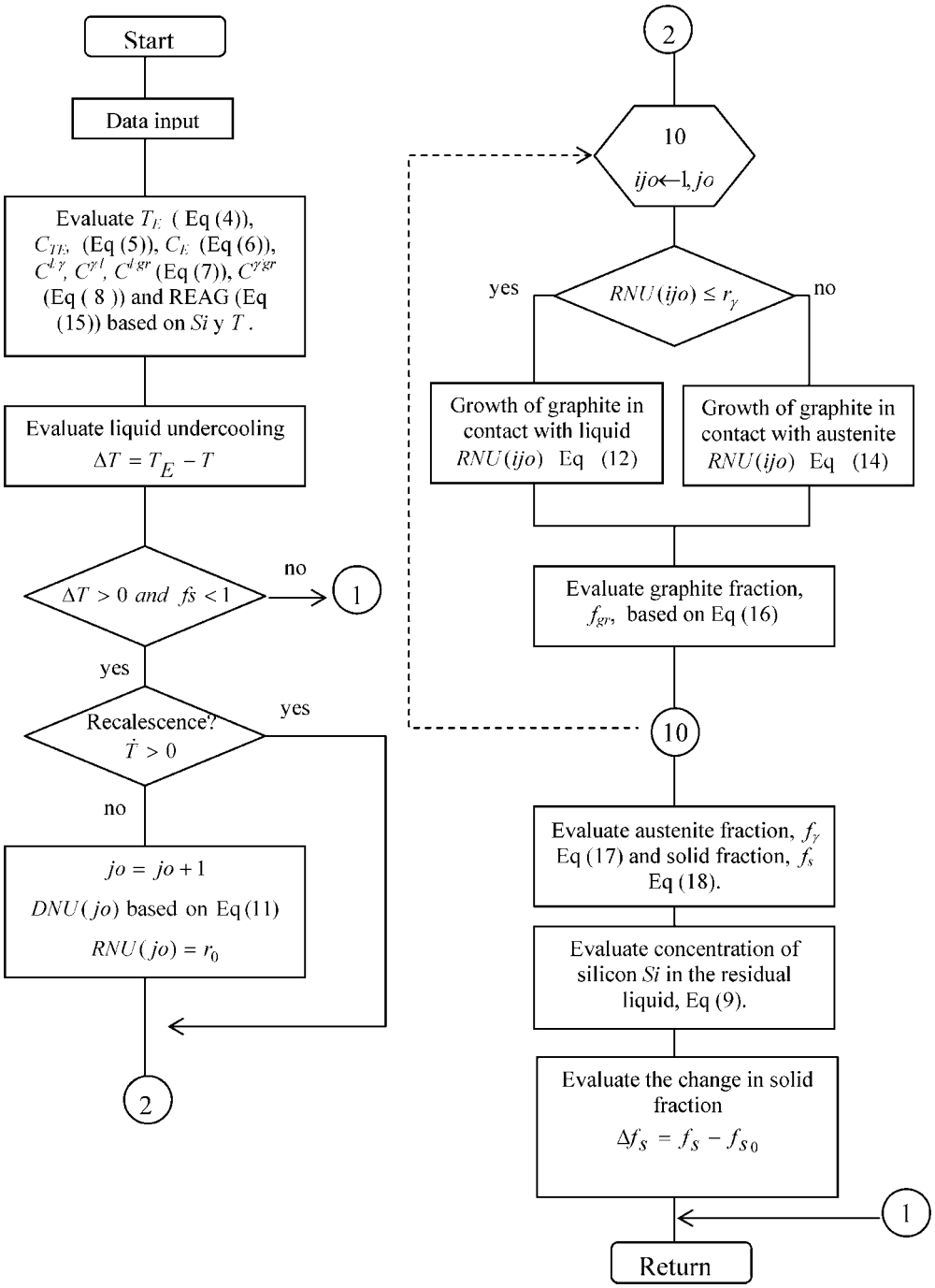

21 Flow diagram used to evaluate microstructural model

the former, with different nucleation laws resulting in differences in recalescence and undercooling. Although it is premature at this stage to make conclusive remarks about the possibilities of those models, the present formulation implemented is capable of serving as a platform for comparison of alternative models and thus investigating their relative merits.

4. Changes in the nucleation conditions in the multinodular model improve the solidification results with respect to the evolution obtained in experiments so that nucleation continues even after recalescence occurs. Moreover, the performance of the model has been assessed under different casting conditions.

Future work in this field should concentrate on improving the simulation of the nucleation and growth of austenite (which was here obtained by the lever rule), since these processes may be of great importance in the multinodular theory. This better representation of austenite can improve the results of cooling curves and solidification times, and also may help to define the transformations within solid state in order to evaluate the final properties of the cast part.

Acknowledgements

This work was supported by the National Technological University (UTN, Facultad Regional Córdoba), the Science and Technology Research Council of Cordoba (Ministerio de Ciencia y Tecnología de Córdoba, Córdoba, Argentina), the Science and Technology Research Council of Argentina (CONICET) and the Chilean Council of Research and Technology

CONICYT (FONDECYT Project No. 1060139). The first author thanks J. Sikora and G. Rivera (INTEMA, Mar del Plata) for their valuable comments on the subject of this paper.

References

1. J. Sikora, R. Boeri and G. Rivera: Proc. Int. Conf. on 'Science of casting and solidification', Brasov, Romania, May 2001, Editura Lux Libris, 321–329.
2. K. Su, I. Ohnaka, I. Yamauchi and T. Fukusako: Proc. 3rd Int. Symp. on 'Metallurgy of cast iron', Stockolm, Sweden, 1984, 181–189.
3. D. M. Stefanescu and D. K. Bandyopadhyay: Proc. 4th Int. Symp. on 'Physical metallurgy of cast iron', Tokyo, Japan, September 1989, 15–26.
4. D. Banerjee and D. Stefanescu: *AFS Trans.*, 1991, **99**, 747–759.
5. R. Boeri and J. Sikora: *Int. J. Cast Metal. Res.*, 2001, **13**, 307–313.
6. E. Fras: Proc. 3rd Int. Symp. on 'Metallurgy of cast iron', Stockolm, Sweden, August 1984, 191–199.
7. H. Fredriksson and I. Svensson: Proc. 3rd Int. Symp. on 'Metallurgy of cast iron', Stockolm, Sweden, August 1984, 273–284.
8. D. Stefanescu and C. Kanetkar: in 'Computer simulation of microstructural evolution', (ed. D. Srolovitz), 171–188; 1985, Toronto, Metallurgical Society Inc.
9. M. Castro, P. Alexandre, J. Lacaze and G. Lesoult: Proc. 4th Int. Symp. on 'Physical metallurgy of cast iron', Tokyo, Japan, September 1989, 433–440.
10. M. I. Onsoien, O. Grong, O. Gundersen and T. Skaland: *Metall. Mater. Trans. A*, 1999, **30A**, 1053–1068.
11. M. I. Onsoien, O. Grong, O. Gundersen and T. Skaland: *Metall. Mater. Trans. A*, 1999, **30A**, 1069–1079.
12. B. C. Liu, H. D. Zhao, W. Y. Liu and D. T. Wang: *Int. J. Cast Metal. Res.*, 1999, **11**, (5), 471–476.
13. H. Zhao and B. Liu: *ISI J. Int.*, 2001, **41**, (9), 986–991.
14. A. Rickert and S. Engler: Proc. 3rd Int. Symp. on 'Metallurgy of cast iron', Stockolm, Sweden, August 1984, 165–174.
15. R. Hummer: Proc. 3rd Int. Symp. on 'Metallurgy of cast iron', Stockolm, Sweden, August 1984, 213–222.
16. R. Boeri: 'The solidification of ductile cast iron', PhD thesis, University of British Columbia, Canada, 1989.
17. J. Sikora, G. Rivera and H. Biloni: Proc. F. Weimberg Int. Symp. on 'Solidification processing', August 1990, Hamilton, Ontario, Pergamon Press, 280–288.
18. G. Rivera, R. Boeri and J. Sikora: *Cast Metals*, 1995, **8**, (1), 1–5.
19. G. Rivera, R. Boeri and J. Sikora: *Adv. Mater. Res.*, 1997, **4**, 169–174.
20. G. Rivera, R. Boeri and J. Sikora: *Int. J. Cast Metal. Res.*, 1999, **11**, (5), 267–272.
21. G. Rivera: 'Estructura de Solidificación de Fundiciones de Hierro con Grafito Esferoidal', Doctoral thesis, National University of Mar del Plata, Mar del Plata, Argentina, 2000, in Spanish.
22. D. Celentano: 'Un Modelo Termomecánico para Problemas de Solidificación de Metales', PhD thesis, Polytechnic University of Catalunya, Barcelona, 1994, in Spanish.
23. D. Celentano, S. Oller and E. Oñate: *Int. J. Solids Struct.*, 1996, **33**, (5), 647–673.
24. R. W. Heine: *AFS Trans.*, 1986, **71**, 391–402.
25. S. Wetterfall, H. Fredriksson and M. Hiller: *J. Iron Steel Inst. I*, 1972, **210I**, 323–333.

Appendix

The computational flow diagram used to evaluate the microstructural model is shown in Fig. 21. The new variables used in the flow chart are: *jo*, the number of different radii of graphite nodules at a Gauss point; *DNU*, the array containing the density of nodules for each nodule size at a Gauss point; *RNU*, the array containing graphite nodules of different radii at a Gauss point; r_0, the initial radius of graphite nodules; r_γ, the radius at which a nodule starts contact with austenite.